Journal of Molecular Science

Journal of Molecular Science
Volume 35 Issue 4, Year of Publication 2025, Page 1748-1756
DoI-10.004687/1000-9035.2025.236

Journal of Molecular Science
www.jmolecularsci.com ISSN:1000-9035

Synthesis, DFT Studies, Molecular Docking and ADMET Predictions of Novel Unsymmetrical Azines

S. Rajapriya[1], R. Arulmani[1*]
[1] PG & Resaerch Dept. of Chemistry, Govt. Arts College, B. Mutlur, Chidambaram (Affiliated to Annamalai University, Annamalai nagar), Tamilnadu, India-608102
Corresponding Author Email: drraulmani@gmail.com

Article Information
Received: 06-08-2025
Revised: 28-09-2025
Accepted: 12-11-2025
Published: 24-12-2025

Keywords
Azine derivative, FT-IR and NMR spectroscopy; Optimization, HOMO–LUMO, NBO analysis, NLO properties, Molecular docking and ADMET predictions.

ABSTRACT
A novel azine derivative, (*1E,2E*)-1-(4-(benzyloxy)benzylidene)-2-(4-nitrobenzylidene)hydrazine, was successfully synthesized and characterized using FT-IR, ^{1}H NMR, and ^{13}C NMR spectral techniques. The spectral data confirmed the formation of the azomethine (C=N) linkage and the presence of benzyloxy and nitro functional groups. Density Functional Theory (DFT) calculations at the B3LYP/6-311++G(d,p) level revealed a nearly planar, conjugated structure with significant intramolecular charge transfer (ICT). Frontier molecular orbital analysis indicated a moderate HOMO–LUMO energy gap (3.026 eV), suggesting good chemical reactivity and stability, while NBO analysis confirmed strong hyperconjugative interactions and efficient charge delocalization across the molecule. The compound exhibited remarkable nonlinear optical (NLO) properties with a first hyperpolarizability significantly higher than urea, indicating its potential in optoelectronic applications. Molecular docking studies against pancreatic α-amylase (1HNY) demonstrated strong binding interactions through hydrogen bonding and hydrophobic contacts, supporting its antidiabetic potential. Furthermore, ADMET analysis revealed good oral bioavailability, high gastrointestinal absorption, non-BBB permeability, and favorable drug-likeness properties, highlighting the compound as a promising candidate for peripheral therapeutic applications.

1. INTRODUCTION:

Azines constitute an important subclass of nitrogen-containing Schiff base derivatives that are typically generated through the condensation reaction between hydrazine and carbonyl compounds such as aldehydes or ketones. These compounds are characterised by the presence of the azine linkage (–C=N–N=C–), which connects two imine groups within a conjugated framework. When the two carbonyl precursors involved in the condensation reaction differ structurally, the resulting molecules are referred to as unsymmetrical azines. The structural asymmetry present in such compounds often leads to enhanced electronic diversity and steric flexibility, thereby expanding their physicochemical properties and potential biological applications compared with symmetrical azine analogues [1,2]. The synthesis of unsymmetrical azines is generally accomplished through a stepwise condensation strategy. In this approach, one aldehyde or ketone first reacts with hydrazine hydrate under controlled stoichiometric conditions to produce a monohydrazone intermediate. This intermediate subsequently undergoes condensation with a second, chemically distinct carbonyl compound to form the desired azine product. Mild acidic catalysts such as glacial acetic acid are frequently employed to promote imine formation

Journal of Molecular Science
Volume 35 Issue 4, Year of Publication 2025, Page 1748-1756
DoI-10.004687/1000-9035.2025.236

and improve reaction yields. In recent years, environmentally friendly synthetic techniques including microwave-assisted reactions, ultrasonic irradiation, and solvent-free conditions have also been explored as efficient alternatives, offering advantages such as reduced reaction time, higher product yield, and lower solvent consumption [3,4]. The incorporation of functional aromatic substituents into the azine framework plays an important role in modulating the electronic behaviour and stability of these molecules. Substituents such as nitrophenyl groups, which possess strong electron-withdrawing characteristics, and benzyloxyphenyl moieties, which act as electron donors through resonance effects, can generate a donor–π–acceptor molecular architecture. This arrangement facilitates intramolecular charge transfer across the conjugated azine bridge and significantly influences the chemical reactivity and biological potential of the resulting compounds [5].

Azine and hydrazone derivatives have attracted considerable attention in medicinal chemistry due to their broad spectrum of pharmacological activities. Numerous studies have reported that such compounds exhibit antimicrobial, antioxidant, anti-inflammatory, anticancer, and antidiabetic properties, largely attributed to the presence of the azomethine (C=N) functional group and the extended π-conjugated system within their structures [6,7]. The search for new antidiabetic agents has become increasingly important due to the rapid rise in the global prevalence of type 2 diabetes mellitus, which currently affects hundreds of millions of individuals worldwide. One promising therapeutic strategy involves the inhibition of carbohydrate-hydrolysing enzymes such as α-amylase and α-glucosidase, as well as other metabolic targets including dipeptidyl peptidase-4 (DPP-4) and protein tyrosine phosphatase 1B (PTP1B). Several azine-based molecules have been reported to exhibit favourable binding interactions and inhibitory activity toward these enzymes, highlighting their potential as antidiabetic drug candidates [8,9]. In addition to experimental investigations, computational chemistry techniques have become essential tools for understanding the structural and electronic properties of organic molecules. Density functional theory (DFT) calculations provide valuable insight into molecular geometry, electronic structure, and chemical reactivity. Analysis of frontier molecular orbitals (HOMO and LUMO) helps in evaluating electron-donating and electron-accepting characteristics as well as chemical stability. Natural bond orbital (NBO) analysis allows the identification of intramolecular charge transfer and hyperconjugative interactions that stabilise the molecular system. Furthermore, the evaluation of nonlinear optical (NLO) parameters, including dipole moment, mean polarizability, and first hyperpolarizability, enables assessment of potential applications in optical materials, particularly for molecules possessing extended conjugated donor–acceptor frameworks [10–12]. Modern drug discovery also relies heavily on in silico pharmacokinetic prediction to evaluate the drug-likeness of newly synthesised compounds before undertaking extensive biological testing. Computational platforms such as SwissADME and pkCSM can predict important ADMET parameters including compliance with Lipinski's rule of five, aqueous solubility, gastrointestinal absorption, blood–brain barrier permeability, metabolic interactions with cytochrome P450 enzymes, and possible toxicity risks. These predictions serve as an efficient preliminary screening step that helps identify promising candidates for further experimental evaluation [13,14]. Although numerous studies have explored the chemistry and biological properties of symmetrical azine derivatives, detailed investigations combining synthetic chemistry, spectroscopic characterisation, density functional theory calculations, molecular docking against antidiabetic targets, and ADMET evaluation for unsymmetrical azines remain relatively limited. Therefore, the present study focuses on the synthesis of the unsymmetrical azine compound (E)-1-(4-(benzyloxy)benzylidene)-2-(4-nitrophenyl)hydrazine, obtained through the condensation of 4-nitrobenzaldehyde, hydrazine hydrate, and 4-benzyloxybenzaldehyde. The synthesised compound was subsequently characterised using spectroscopic techniques and further investigated through DFT-based electronic structure analysis, molecular docking studies, and ADMET prediction in order to explore its potential as a promising antidiabetic candidate and to establish structure–activity relationships within this class of compounds [15].

2. Experimental

2.1 Materials and Chemicals

All chemicals used in this study were of analytical reagent (AR) grade and were used as received without further purification. 4-Nitrobenzaldehyde, hydrazine hydrate (99%), 4-benzyloxybenzaldehyde, and glacial acetic acid were procured from Sigma-Aldrich/TCI Japan Chemical Company, Bangalore- 560100, India. Absolute ethanol (99.9%) used as the reaction solvent was sourced from the same supplier. Thin-layer chromatography (TLC) was performed on Merck silica gel 60 F_{254} aluminium sheets, and spots were visualised under UV light (254/365 nm). Melting points were determined using an open capillary method on a digital melting-point apparatus and are uncorrected.

Journal of Molecular Science
Volume 35 Issue 4, Year of Publication 2025, Page 1748-1756
DoI-10.004687/1000-9035.2025.236

2.2 Synthesis of (1E,2E)-1-(4-(benzyloxy) benzylidene)-2-(4-nitrobenzylidene) hydrazine

The title unsymmetrical azine was synthesised via a stepwise condensation approach. In the first step, 4-benzyloxybenzaldehyde (0.01 mol) and hydrazine hydrate (0.01 mol, 5 mL) were placed in a stoppered conical flask. The mixture was dissolved in absolute ethanol and stirred at room temperature for approximately 30 min. The intermediate monohydrazone, *(E)-(4-(benzyloxy) benzylidene) hydrazine* **(2)**, separated as a white solid and was stirred with 4-nitrobenzaldehyde (0.01 mol) in ethanol containing a catalytic amount of glacial acetic acid [16]. The progress of the reaction was monitored continuously by TLC (ethyl acetate/hexane, 3:7 v/v). Upon completion, the reaction mixture was cooled to room temperature, and the yellow solid that separated was collected by filtration, washed with cold ethanol, and recrystallised from ethanol to afford the pure target compound **(Scheme 1)**.

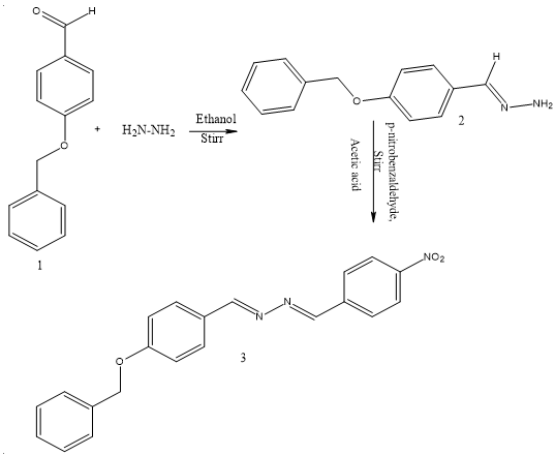

Scheme 1. **Stepwise synthesis of (*1E,2E*)-1-(4-(benzyloxy) benzylidene)-2-(4-nitrobenzylidene) hydrazine**

3. RESULTS AND DISCUSSION:

3.1 Spectral data

Mp : 132-133°C; Pale yellow solid; Yield-79%; IR(νcm^{-1}); **IR (KBr disc, cm^{-1}) (2):** 3443 (ν N–H stretching, hydrazone), 3106, 3046 (ν Ar–C–H stretching), 2925 (ν C–H stretching, –OCH_2–), 1692 (ν C=N stretching, azomethine), 1603, 1576 (ν C=C stretching, aromatic), 1538, 1511 (ν NO_2 asymmetric stretching), 1386, 1349 (ν NO_2 symmetric stretching), 1258 (ν C–O–C symmetric stretching, aryl ether), 1162 (ν C–N stretching, hydrazone), 1105 (ν C–O stretching, benzyloxy), 857, 822 (δ C–H out-of-plane bending, *para*-disubstituted ring), 736, 690 (δ C–H out-of-plane bending, monosubstituted phenyl) cm^{-1}.

IR (KBr disc, cm^{-1}) (3): 3004 (ν Ar–C–H stretching), 2948, 2907, 2833 (ν C–H stretching, aliphatic –OCH_2–), 1618 (ν C=N stretching, azomethine), 1491 (ν NO_2 asymmetric stretching), 1461 (δ C–H scissoring, –CH_2–), 1421 (ν C=C stretching, aromatic), 1331 (ν NO_2 symmetric stretching), 1259 (ν C–O–C asymmetric stretching, aryl ether), 1219 (ν C–N stretching), 1159 (ν C–O stretching, benzyloxy), 1040 (ring breathing), 954 (δ C–H out-of-plane bending), 813 (δ C–H out-of-plane bending, *para*-disubstituted ring), 705 (δ C–H out-of-plane bending, monosubstituted phenyl) cm^{-1}.

^{1}H NMR (500 MHz, $CDCl_3$) (3): δppm 9.884 (s, 1H, N=C**H**, azomethine), 8.404 (d, 2H, Ar–H, *p*-NO_2 phenyl, *ortho* to NO_2), 8.084–8.067 (d, 2H, Ar–H, *p*-NO_2 phenyl, *meta* to NO_2), 7.847–7.830 (d, 2H, Ar–H, benzyloxy phenyl, *ortho* to CH=N), 7.441–7.420 (m, 2H, Ar–H, benzyl –Ph), 7.418–7.401 (m, 2H, Ar–H, benzyl –Ph), 7.389–7.369 (m, 1H, Ar–H, benzyl –Ph, *para*), 7.366–7.352 (d, 2H, Ar–H, benzyloxy phenyl, *ortho* to OCH_2), 7.357–7.338 (overlap, 2H), 7.260 (s, residual $CDCl_3$), 7.088–7.071 (d, 2H, Ar–H), 5.152 (s, 2H, O–C**H_2**–Ph, benzyl –CH_2) ppm. **^{13}C NMR (125 MHz, $CDCl_3$) (3)**: δ 163.75 (C–O, *ipso*-benzyloxy), 151.14 (C–N, *ipso*-nitrophenyl), 140.05 (C=N, azomethine), 135.95 (C–NO_2), 132.03 (C–CH=N, *ipso*-benzyloxyphenyl), 130.51, 130.12, 128.76, 128.36, 127.51, 124.33, 115.16 (Ar–CH), 70.28 (–OCH_2–) ppm.

3.2 DFT analysis:

3.2.1 Geometry Optimization and Molecular Structure:

The ground-state geometry of **(1E,2E)-1-(4-(benzyloxy) benzylidene)-2-(4-nitrobenzylidene) hydrazine** was fully optimized as shown in **Figure-1** using density functional theory (DFT) at the B3LYP/6-311++G(d,p) level of theory as implemented in the Gaussian 09 software package [18]. The B3LYP functional, which combines Becke's three-parameter hybrid exchange functional with the Lee–Yang–Parr correlation functional [19], has been widely validated for the accurate prediction of molecular geometries, vibrational frequencies, and electronic properties of Schiff base and hydrazone–azine derivatives [20]. The azine core is defined by the two imine bonds displayed in **Table-1**, C1=N15 and C18=N17, with bond lengths of 1.3023 Å and 1.2974 Å respectively, which are characteristic of C=N double bond character (typical range: 1.270–1.310 Å) and confirm the fully conjugated bis-imine –C=N–N=C– linkage [20]. The central N15–N17 single bond length of 1.4200 Å is consistent with an N–N bond possessing partial double bond character arising from delocalisation across the azine bridge, and is in good agreement with values reported for related hydrazone–azine systems [21]. The C1–C2 bond (1.4517 Å) connecting the azomethine carbon to the benzyloxyphenyl ring is slightly elongated

Journal of Molecular Science
Volume 35 Issue 4, Year of Publication 2025, Page 1748-1756
DoI-10.004687/1000-9035.2025.236

compared to a typical aromatic C–C bond (~1.395 Å), reflecting the cross-conjugation between the ring and the C=N unit. Within the benzyloxyphenyl ring, the C–C bond lengths range from 1.3850 to 1.4163 Å, consistent with aromatic delocalization, while the aryl ether C9–O11 bond (1.3836 Å) and the O11–C12 bond (1.4708 Å) are in excellent agreement with reported Ar–O and O–CH_2 bond lengths in benzyloxy-substituted aromatics [22]. The benzyl methylene C12–C31 bond (1.5043 Å) is a typical sp^3–sp^2 C–C single bond, and the pendant monosubstituted phenyl ring (C31–C38) displays uniform aromatic C–C bond lengths of 1.397–1.405 Å. On the electron-withdrawing terminus, the nitro group N42–O43 and N42–O44 bond lengths of 1.2658 Å and 1.2660 Å are nearly equivalent, confirming symmetric electron delocalisation within the –NO_2 group, and the C24–N42 bond (1.4623 Å) reflects the single-bond character between the aromatic ring and the nitro nitrogen. The C23–C24 bond angle at N42 is 119.06°, and the O–N–O angle defined by O43–N42–O44 is consistent with the reported range of 123–125° for aromatic nitro groups [22]. The dihedral angle analysis reveals that the central azine bridge adopts a nearly planar trans–trans (E,E) conformation: the dihedral C2–C1–N15–N17 of approximately 179.80° and N15–N17–C18–C20 of approximately 179.81° confirm the *E*-configuration about both C=N bonds, in full agreement with the ^{1}H NMR data. The near-zero dihedral angles within the nitrophenyl ring (e.g., C22–C23–C24–N42 = 179.99°) confirm coplanarity of the nitro group with the aromatic ring, maximising resonance withdrawal. Collectively, the optimized geometric parameters demonstrate that the molecule adopts an extended, near-planar conformation across the entire donor–π–bridge–acceptor framework, which is a prerequisite for significant intramolecular charge transfer (ICT) and nonlinear optical (NLO) activity [23].

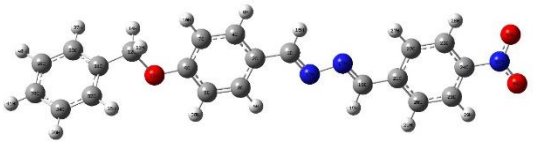

Figure-1. Optimized geometry

Table-1. Optimized bond parameters

Bond length (A)		Bond Angle ()		Dihedral Angle	
C1-C2	1.452	C1-C2-C3	121.865	C3-C1-C2-C4	-179.979
C2-C3	1.416	C1-C2-C4	119.586	C1-C2-C3-C5	179.938
C2-C4	1.407	C2-C3-C5	120.631	H1-H2-H3-H6	-0.046
C3-C5	1.385	H2-H3-H6	118.572	C1-C2-C4-C7	-179.945
H3-H6	1.084	C2-C4-C7	121.310	H1-H2-H4-H8	0.100
C4-C7	1.397	H2-H4-H8	119.392	C2-C4-C7-C9	0.047
H4-H8	1.086	C4-C7-C9	119.223	H2-H4-H7-H10	-179.838
C7-C9	1.403	H4-H7-H10	119.587	O4-O7-O9-O11	179.961
H7-H10	1.083	O7-O9-O11	124.498	C7-C9-C11-C12	-1.719
O9-O11	1.384	C9-C11-C12	119.305	H9-H11-H12-H13	-57.089
C11-C12	1.471	H11-H12-H13	108.272	H9-H11-H12-H14	61.057
H12-H13	1.098	H11-H12-H14	109.459	N4-N2-N1-N15	179.798
H12-H14	1.096	N2-N1-N15	122.282	H2-H15-H1-H16	179.970
N1-N15	1.302	H15-H1-H16	119.619	N2-N1-N15-N17	-179.965
H1-H16	1.093	N1-N15-N17	112.247	C1-C15-C17-C18	179.815
N15-N17	1.420	C15-C17-C18	112.964	H15-H17-H18-H19	-0.003
C17-C18	1.297	H17-H18-H19	120.184	C15-C17-C18-C20	-179.897
H18-H19	1.092	C17-C18-C20	151.266	C17-C18-C20-C21	-0.134
C18-C20	2.477	C18-C20-C21	30.952	C18-C20-C21-C22	179.971
C20-C21	1.410	C20-C21-C22	119.172	C20-C21-C22-C23	-0.010
C21-C22	1.413	C21-C22-C23	120.522	C21-C22-C23-C24	0.003
C22-C23	1.390	C22-C23-C24	118.913	C17-C18-C20-C25	-0.063
C23-C24	1.401	C18-C20-C25	151.762	H17-H18-H20-H26	179.883
C20-C25	1.393	H18-H20-H26	88.582	H20-H21-H22-H27	179.993
H20-H26	1.085	H21-H22-H27	118.613	H21-H22-H23-H28	179.991
H22-H27	1.083	H22-H23-H28	121.704	H18-H20-H25-H29	179.955
H23-H28	1.082	H20-H25-H29	121.827	H2-H3-H5-H30	179.987
H25-H29	1.082	H3-H5-H30	121.678	C9-C11-C12-C31	-177.912
H5-H30	1.083	C11-C12-C31	108.003	C11-C12-C31-C32	60.943
C12-C31	1.504	C12-C31-C32	120.225	C11-C12-C31-C33	-119.429
C31-C32	1.405	C12-C31-C33	120.595	C12-C31-C32-C34	179.525
C31-C33	1.402	C31-C32-C34	120.375	H12-H31-H32-H35	-1.278
C32-C34	1.397	H31-H32-H35	119.448	C12-C31-C33-C36	-179.131
H32-H35	1.085	C31-C33-C36	120.517	H12-H31-H33-H37	1.043
C33-C36	1.400	H31-H33-H37	119.619	C31-C33-C36-C38	-0.485
H33-H37	1.086	C33-C36-C38	119.977	H31-H32-H34-H39	179.795
C36-C38	1.399	H32-H34-H39	119.852	H31-H33-H36-H40	179.907
H34-H39	1.085	H33-H36-H40	119.856	H33-H36-H38-H41	-179.812
H36-H40	1.085	H36-H38-H41	120.110	N22-N23-N24-N42	179.990

Journal of Molecular Science
Journal of Molecular Science
Volume 35 Issue 4, Year of Publication 2025, Page 1748-1756
DoI-10.004687/1000-9035.2025.236

H38-H41	1.085	N23-N24-N42	119.064	O23-O24-O42-O43	-0.012
N24-N42	1.462	O24-O42-O43	118.122	O23-O24-O42-O44	179.990
O42-O43	1.266	O24-O42-O44	118.146		
O42-O44	1.266				

3.2.2 Frontier molecular orbital analysis

The frontier molecular orbital energies, global reactivity descriptors, and electron density distributions of titled compound computed at the B3LYP/6-311++G(d,p) level are presented in **Table-2** and **Figure-2**. The HOMO energy of −6.069 eV and LUMO energy of −3.043 eV afford a HOMO–LUMO energy gap (ΔE) of 3.026 eV, which serves as a key indicator of the kinetic stability and chemical reactivity of the molecule, the relatively narrow energy gap is attributed to the extended π-conjugation across the donor–π–acceptor framework, from the electron-donating 4-benzyloxyphenyl group through the –C=N–N=C– azine bridge to the electron-withdrawing 4-nitrophenyl terminus, which facilitates efficient intramolecular charge transfer (ICT) and renders the molecule chemically soft, polarisable, and reactive towards both electrophilic and nucleophilic interactions [24]. This ICT character is vividly confirmed by the spatial distribution of the frontier orbitals: in the HOMO, electron density is predominantly delocalised over the central azine bridge and the benzyloxyphenyl aromatic ring (C2–C9, N15, N17, C18, C20–C25), with substantial π-orbital contributions extending partially onto the nitrophenyl ring and its oxygen atoms, while the pendant benzyl group (C31–C38) and the –OCH_2– methylene (C12) remain essentially devoid of HOMO density; in sharp contrast, the LUMO electron density is strongly concentrated on the electron-withdrawing 4-nitrophenyl half of the molecule that on the nitrophenyl ring (C20–C25), the azine nitrogen atoms (N15, N17), the C18 azomethine carbon, and the nitro group (N42, O43, O44) with negligible contribution from the benzyloxyphenyl ring and benzyl group, providing unambiguous visual evidence for electron density migration from the donor to the acceptor terminus upon electronic excitation [25]. The ionization energy (I = 6.069 eV) and electron affinity (A = 3.043 eV) derived via Koopmans' theorem reflect the stability of the HOMO and the strong electron-accepting capacity of the LUMO respectively, the latter being consistent with the significant lowering of LUMO energy by the *p*-nitro group. From the global reactivity descriptors, the global hardness (η = 1.513 eV) confirms the soft nature of the molecule while the chemical softness (S = 0.661 eV) corroborates its high polarisability; the electronegativity (χ = 4.556 eV) and chemical potential (μ = −4.556 eV) indicate a moderate electron-attracting tendency, and the high electrophilicity index (ω = 6.860 eV) classifies titled compound as a strong electrophile according to the scale proposed by Domingo et al., suggesting a strong capacity to accept electron density from biological nucleophiles at enzyme active sites, which may underpin its antidiabetic activity [26, 27].

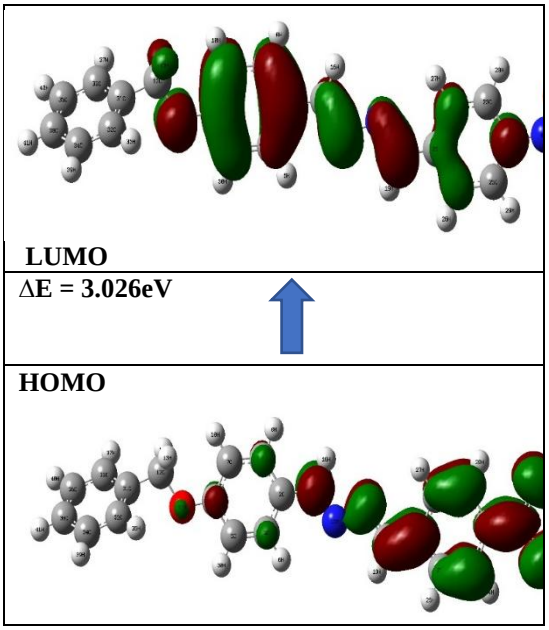

Figure-2. FMO orbitals

Table-2. Electronic and Global descriptors

Electronic Parameters	eV	Global reactivity parameters	eV
E_{Homo}(a u)	-6.069	Global hardness(η)	1.513
E_{Lumo}(a.u)	-3.043	Chemical potential(μ)	-4.556
Energy gap(a.u)	3.026	Electrophilicity index(ω)	6.860
Ionization energy(I)	6.069	Chemical softness(s)	0.661
Electron affinity(A)	3.043	Electronegativity (χ)	4.556

3.2.3 NBO analysis

The second-order perturbation theory analysis of the Fock matrix within the NBO basis, performed at the B3LYP/6-311++G(d,p) level, provides detailed insight into the hyperconjugative interactions, charge delocalisation, and intramolecular charge transfer (ICT) pathways in titled compound; the stabilisation energies $E^{(2)}$ for all significant donor–acceptor interactions are listed in **Table-3** [28]. The most dominant interaction in the entire molecule is the lone pair donation from oxygen O44 into the π*(N42–O43) antibonding orbital with a remarkably

Journal of Molecular Science
Volume 35 Issue 4, Year of Publication 2025, Page 1748-1756
DoI-10.004687/1000-9035.2025.236

high E(2) value of 730.150 kJ/mol, reflecting the strong resonance delocalisation within the nitro group (–NO_2) and confirming the near-equivalent N–O bond lengths (1.2658 and 1.2660 Å) observed in the optimised geometry; this is further supported by the O43 → σ*(N42–O44) and O44 → σ*(C24–N42) interactions (E(2) = 77.446 and 42.342 kJ/mol respectively), collectively demonstrating the extensive electron delocalisation within the *p*-nitrophenyl terminus [29]. The second most significant interaction is the lone pair donation from the benzyloxy oxygen O11 into the π*(C7–C9) antibonding orbital (E(2) = 130.457 kJ/mol), which confirms the strong mesomeric electron donation of the –OCH_2– aryl ether oxygen into the benzyloxyphenyl ring, consistent with its role as the principal electron-donating group driving ICT across the azine framework [29]. Within the benzyloxyphenyl ring, extensive π→π* delocalisation is evidenced by interactions such as C7–C9(π) → C2–C4(π*) (E(2) = 96.567 kJ/mol), C2–C4(π) → C1–N15(π*) (E(2) = 97.655 kJ/mol), and C3–C5(π) → C7–C9(π*) (E(2) = 94.768 kJ/mol), confirming efficient conjugation between the aromatic ring and the azomethine C1=N15 bond; the C1–N15(π) → N17–C18(π*) interaction ($E^{(2)}$ = 56.400 kJ/mol) and the reciprocal N17–C18(π) → C1–N15(π*) interaction (E(2) = 46.191 kJ/mol) together confirm the delocalisation across the central –C=N–N=C– azine bridge, establishing a continuous conjugation pathway from the donor to the acceptor terminus [11]. On the acceptor side, the nitrophenyl ring participates in strong π→π* interactions including C20–C21(π) → C24–C25(π*) ($E^{(2)}$ = 100.207 kJ/mol) and C24–C25(π) → N42–O43(π*) (E(2) = 146.524 kJ/mol), the latter representing the critical charge transfer from the nitrophenyl ring π-system into the nitro group antibonding orbital and confirming the effective electron-withdrawing resonance of the –NO_2 group. The pendant benzyl phenyl ring (C31–C38) also displays characteristic aromatic π→π* hyperconjugation with $E^{(2)}$ values ranging from 82.550 to 86.818 kJ/mol for C31–C33(π)/C32–C34(π)/C36–C38(π) interacting pairs, consistent with typical benzene ring delocalisation energies but lower than those of the electronically perturbed rings, confirming the relatively isolated electronic character of the benzyl group. Taken together, the NBO analysis establishes a well-defined ICT pathway: O11(n) → benzyloxyphenyl ring → C1=N15 → N15–N17 → C18=N17 → nitrophenyl ring → NO_2, with the highest stabilisation energies concentrated at the donor oxygen and acceptor nitro termini, fully corroborating the FMO electron density distribution and the narrow HOMO–LUMO gap of 3.026 eV.

Table-3 NBO transions and energies

Donor		Acceptor		$E^{(2)}$ Kj/mol
C 1 - N 15	π	N 17 - C 18	π*	56.400
C 2 - C 4	π	C 1 - N 15	π*	97.655
C 2 - C 4	π	C 3 - C 5	π*	82.383
C 2 - C 4	π	C 7 - C 9	π*	74.266
C 3 - C 5	π	C 2 - C 4	π*	69.705
C 3 - C 5	π	C 7 - C 9	π*	94.768
C 7 - C 9	π	C 2 - C 4	π*	96.567
C 7 - C 9	π	C 3 - C 5	π*	61.128
N 17 - C 18	π	C 1 - N 15	π*	46.191
N 17 - C 18	π	C 20 - C 21	π*	43.681
C 20 - C 21	π	N 17 - C 18	π*	76.191
C 20 - C 21	π	C 22 - C 23	π*	71.379
C 20 - C 21	π	C 24 - C 25	π*	100.207
C 22 - C 23	π	C 20 - C 21	π*	87.153
C 22 - C 23	π	C 24 - C 25	π*	86.065
C 24 - C 25	π	C 20 - C 21	π*	75.103
C 24 - C 25	π	C 22 - C 23	π*	79.161
C 24 - C 25	π	N 42 - O 43	π*	146.524
C 31 - C 33	π	C 32 - C 34	π*	83.094
C 31 - C 33	π	C 36 - C 38	π*	83.764
C 32 - C 34	π	C 31 - C 33	π*	86.818
C 32 - C 34	π	C 36 - C 38	π*	85.939
C 36 - C 38	π	C 31 - C 33	π*	86.232
C 36 - C 38	π	C 32 - C 34	π*	82.550
O 11	n	C 7 - C 9	π*	130.457
O 43	n	C 24 - N 42	σ*	42.342
O 43	n	N 42 - O 44	σ*	77.446
O 44	n	C 24 - N 42	σ*	42.342
O 44	n	N 42 - O 43	π*	730.150

3.2.4 NLO analysis

The NLO properties of titled compound computed at the B3LYP/6-311++G(d,p) level and compared with urea (μ = 1.373 Debye, ⟨α⟩ = 3.831 a.u., β_0 = 0.3728 × 10^{-30} esu) as standard reference are summarised in **Table-4**, the total dipole moment μ_{tot} = 6.004 Debye (4.4 × urea), dominated by μ_x = 5.961 Debye along the principal ICT axis, confirms the strongly asymmetric charge distribution across the 4-benzyloxyphenyl donor of azine bridge via 4-nitrophenyl acceptor framework [12]. The mean polarisability ⟨α⟩ = 170.462 a.u. (α_{tot} = 25.262 × 10^{-24} esu) with dominant component α_{xx} = 211.207 a.u. reflects the high deformability of the extended π-conjugated bis-imine system along the molecular long axis, while the predominant tensor contributions β_{xxx} = 1021.503 a.u. and β_{xxy} = 64.813 a.u. confirm that the hyperpolarisability response is overwhelmingly one-dimensional along the donor–acceptor ICT direction [30]. The first hyperpolarisability β_0 = 9.207 × 10^{-30} esu (β_{tot} = 1065.704 a.u.), being approximately 24.7 times greater than urea, unambiguously classifies titled compound as a strongly active second-order NLO chromophore, with the exceptional response arising from the synergistic electron donation of the benzyloxy oxygen, the extended azine π-bridge conjugation, and the powerful electron-withdrawing nitro group, collectively establishing its potential for photonic and electro-optic applications [31].

Table-4 NLO parameters

Dipolemoment		Hyperpolarizability	
μ_x	5.961	β_{xxx}	1021.5

Journal of Molecular Science
Volume 35 Issue 4, Year of Publication 2025, Page 1748-1756
DoI-10.004687/1000-9035.2025.236
Journal of Molecular Science

μ_y	-0.37	β_{xxy}	64.813
μ_z	0.614	β_{xyy}	44.317
μ_{tot} (Debye)	6.004	β_{yyy}	1.745
Polarizability		β_{xxz}	6.422
α_{xx}	-211.21	β_{xyz}	0.626
α_{xy}	-17.64	β_{yyz}	-0.186
α_{yy}	-134.85	β_{xzz}	-2.217
α_{xz}	5.334	β_{yzz}	0.095
α_{yz}	0.886	β_{zzz}	-0.762
α_{zz}	-165.33	β_{tot} (a.u)	1065.7
$<\alpha>$ (a.u)	170.462	β_o(esu) x 10^{-30}	9.206
α_{tot} (esu) x 10^{-24}	25.262		

3.3 Molecular Doking with 1HNY

The molecular docking analysis has been evaluated using Autodock tools [32] with the protein pancreatic alpha-amylase enzyme (pdb id : 1HNY) [33]and the results revealed that the ligand forms several stabilizing interactions as shown in **Figure-3**, within the active site of the target protein. Three **conventional hydrogen bonds** as displayed in **Table-5** were observed with **GLN63** and **LYS200** residues at distances of 3.29, 3.21, and 3.03 Å, indicating strong ligand–protein binding. A **π–donor hydrogen bond** with **TYR151** (3.88 Å) further contributes to the stability of the complex. In addition, multiple **hydrophobic interactions**, including π–σ with **LEU165**, π–π stacked interactions with **TYR151**, π–π T-shaped interaction with **HIS201**, and π–alkyl contacts, enhance the binding affinity of the ligand within the active site. These interactions collectively suggest favorable stabilization of the ligand–protein complex.

Table-5 Molecular docking results with ligand and 1hny

Amino acid residue	Distance between residue and ligand (A)	Name of Interaction	Type of interaction
GLN63	3.292	Hydrogen Bond	Conventional Hydrogen Bond
GLN63	3.210	Hydrogen Bond	Conventional Hydrogen Bond
LYS200	3.040	Hydrogen Bond	Conventional Hydrogen Bond
TYR151	3.888	Hydrogen Bond	Pi-Donor Hydrogen Bond
LEU165	3.772	Hydrophobic	Pi-Sigma
TYR151	5.261	Hydrophobic	Pi-Pi Stacked
TYR151	4.206	Hydrophobic	Pi-Pi Stacked
HIS201	5.208	Hydrophobic	Pi-Pi T-shaped
ILE235	5.338	Hydrophobic	Pi-Alkyl
LEU162	5.362	Hydrophobic	Pi-Alkyl

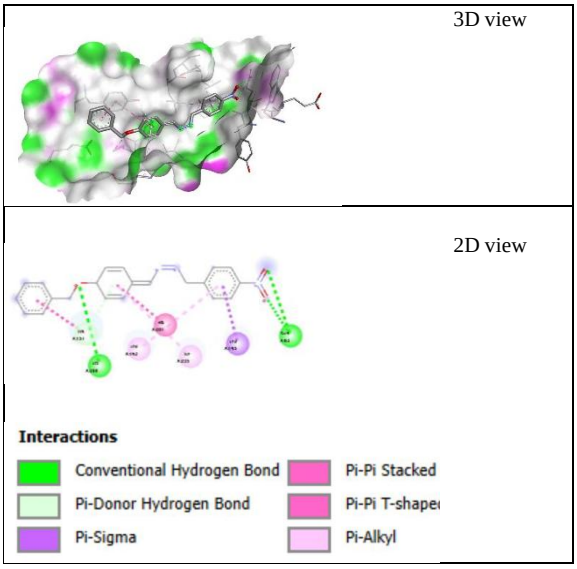

Figure-3. 3D and 2D view interaction with 1hny protease

3.4 ADMEt prediction:

The drug-likeness and pharmacokinetic properties of titled compound were evaluated using the SwissADME online tool [13], and the results are presented in **Table-5** along with the bioavailability radar (**Figure-4**) and BOILED-Egg plot (**Figure-5**). Titled compound (MW = 359.38 g/mol, MF = $C_{21}H_{17}N_3O_3$) fully satisfies Lipinski's Rule of Five with zero violations, MW < 500, consensus log P (3.93) < 5, H-bond acceptors (5) ≤ 10, and H-bond donors (0) ≤ 5, confirming excellent predicted oral bioavailability, further supported by a bioavailability score of 0.55 and zero violations across all additional drug-likeness filters (Ghose, Veber, Egan, and Muegge) [34, 35]. The topological polar surface area (TPSA = 79.77 Ų) and the number of rotatable bonds (7) satisfy Veber's criteria (TPSA ≤ 140 Ų, rotatable bonds ≤ 10) for good oral absorption, and the high GI absorption prediction confirms favourable gastrointestinal permeability; however, titled compound is predicted to be a non-BBB permeant, consistent with its moderate TPSA value, suggesting CNS penetration is unlikely and supporting selective peripheral antidiabetic activity [36]. The consensus log P of 3.93, corroborated by $i_{LOG}P$ (3.30), $X_{LOG}P3$ (4.59), $W_{LOG}P$ (4.47), $M_{LOG}P$ (3.70), and Silicos-IT log P (3.56), indicates moderate lipophilicity within the optimal range (1 < log P < 5) for drug-like molecules, while the aqueous solubility predictions classify titled compound as moderately soluble by both E_{SOL} (log S = −4.99, 3.67 × 10^{-3} mg/mL) and Ali methods (log S = −5.99) and poorly soluble by Silicos-IT (log S = −7.10), suggesting that formulation strategies may be required to optimise bioavailability. Regarding metabolism, titled compound is predicted to inhibit CYP1A2 and CYP2C19 but not CYP2C9, CYP2D6, or CYP3A4, indicating a selective cytochrome P450 inhibition profile that warrants consideration in

Journal of Molecular Science
Journal of Molecular Science
Volume 35 Issue 4, Year of Publication 2025, Page 1748-1756
DoI-10.004687/1000-9035.2025.236

combination therapy contexts; the skin permeability log Kp = −5.23 cm/s indicates low dermal penetration, the molecular refractivity (MR = 107.87) falls within the Ghose filter range, and the synthetic accessibility score of 2.81 (scale 1–10) confirms that titled compound is readily synthesisable. The bioavailability radar plot (Fig. 3) shows that all six physicochemical parameters like LIPO, SIZE, POLAR, INSOLU, INSATU and FLEX are fall within or close to the optimal pink shaded region, with high lipophilicity (LIPO) and moderate flexibility (FLEX) as the most prominent features, while zero PAINS alerts and three Brenk alerts (with two leadlikeness violations) indicate an acceptable safety and lead-likeness profile for further antidiabetic drug development [37, 38]. The BOILED-Egg model shows that the compound lies in the white region, indicating **good human intestinal absorption (HIA)** but no blood–brain barrier (BBB) penetration. It is also predicted to be **non-substrate of P-glycoprotein (PGP⁻)**, suggesting favorable bioavailability without active efflux.

Table-6 ADMET predcition data by Swiss ADME tool

ADMET predictions			
Formula	$C_{21}H_{17}N_3O_3$	Silicos-IT Solubility (mg/ml)	2.87
MW	359.38	Silicos-IT Solubility (mol/l)	8
Fraction Csp3	0.05	Silicos-IT class	Poorly soluble
Rotatable bonds	7	GI absorption	High
H-bond acceptors	5	BBB permeant	No
H-bond donors	0	Pgp substrate	No
MR	107.87	CYP1A2 inhibitor	Yes
TPSA	79.77	CYP2C19 inhibitor	Yes
$i_{LOG}P$	3.3	CYP2C9 inhibitor	No
$X_{LOG}P3$	4.59	CYP2D6 inhibitor	No
$W_{LOG}P$	4.47	CYP3A4 inhibitor	No
$M_{LOG}P$	3.7	log Kp (cm/s)	-5.23
Silicos-IT Log P	3.56	Lipinski violations	0
Consensus Log P	3.93	Ghose violations	0
E_{SOL} Log S	-4.99	Veber violations	0
E_{SOL} Solubility (mg/ml)	3.67	Egan violations	0
E_{SOL} Solubility (mol/l)	1.02	Muegge violations	0
ESOL Class	Moderately soluble	Bioavailability Score	0.55
Ali Log S	-5.99	PAINS alerts	0
Ali Solubility (mg/ml)	3.68	Brenk alerts	3
Ali Solubility (mol/l)	1.02	Leadlikeness violations	2
Ali Class	Moderately soluble	Synthetic Accessibility	2.81
Silicos-IT LogSw	-7.1		

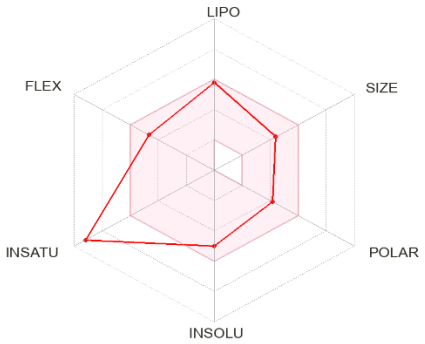

Figure-4 Bioavailability radar prediction

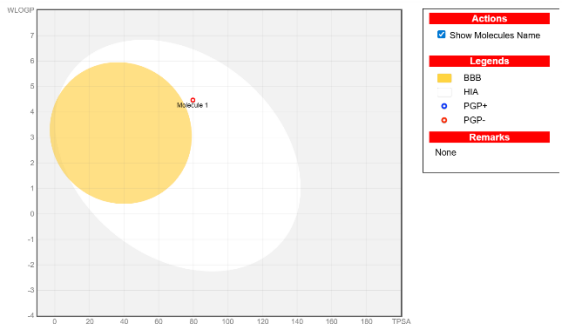

Figure-5 Boiled-egg model

CONCLUSION:

The present study successfully established the synthesis, structural characterization, and computational evaluation of a novel azine-based compound with a donor–π–acceptor framework. Spectroscopic analysis confirmed the molecular structure, while DFT studies revealed a planar geometry conducive to effective conjugation and charge transfer. The moderate HOMO–LUMO energy gap and strong electrophilic nature indicate good reactivity and stability. NBO and NLO

Journal of Molecular Science
Volume 35 Issue 4, Year of Publication 2025, Page 1748-1756
DoI-10.004687/1000-9035.2025.236

analyses demonstrated significant electron delocalization and excellent nonlinear optical response, emphasizing its potential in advanced material applications. Molecular docking results confirmed strong interactions with key active site residues of α-amylase, suggesting promising antidiabetic activity. ADMET predictions further supported its drug-likeness, good gastrointestinal absorption, and safe pharmacokinetic profile. Overall, the combined experimental and theoretical findings suggest that the titled compound is a potential candidate for both pharmaceutical and optoelectronic applications, warranting further biological and experimental investigations.

AUTHOR CONTRIBUTIONS:

Conceptualization, Synthesis, Molecular modeling, Writing, Original Draft Preparation – **S. Rajapriya**; Writing, Review & Editing, Enzyme inhibition assays, Supervision and Project Administration – **R. Arulmani**.

Funding: This research has no funding.

Conflicts of Interest: The authors declare no conflict of interest.

REFERENCES:

1. Rollas, S.; Küçükgüzel, Ş. G.*Molecules* **2007**, *12*, 1910–1939.
2. Küçükgüzel, İ.; Tatar, E.; Küçükgüzel, Ş. G.; Rollas, S.; De Clercq, E.*Eur. J. Med. Chem.* **2013**, *69*, 691–700.
3. Ajani, O. O.; Obafemi, C. A.; Nwinyi, O. C.; Akinpelu, D. A.*J. Mol. Struct.* **2019**, *1177*, 724–735.
4. Tanaka, K.; Toda, F.*Chem. Rev.* **2000**, *100*, 1025–1074.
5. Mahmoud, W. H.; Deghadi, R. G.; Mohamed, G. G.; El-Gamel, N. E. A.*Spectrochim. Acta A* **2018**, *191*, 591–600.
6. Kumar, S.; Dhar, D. N.; Saxena, P. N.*J. Sci. Ind. Res.* **2009**, *68*, 181–187.
7. da Silva, C. M.; da Silva, D. L.; Modolo, L. V.; Alves, R. B.; de Resende, M. A.; Martins, C. V. B.; de Fátima, Â.*J. Adv. Res.* **2011**, *2*, 1–8.
8. International Diabetes Federation. *Diabetes Res. Clin. Pract.* **2022**, *183*, 109119.
9. Durdagi, S.; Dag, C.; Dogan, B.; Yigin, M.; Avsar, T.; Buyukdagli, S. *Bioorg. Med. Chem. Lett.* **2016**, *26*, 2273–2278.
10. Parr, R. G.; Yang, W. *Annu. Rev. Phys. Chem.* **1995**, *46*, 701–728.
11. Reed, A. E.; Weinhold, F. *J. Chem. Phys.* **1985**, *83*, 1736–1740.
12. Prasad, P. N.; Williams, D. J. *Chem. Rev.* **1991**, *91*, 157–191.
13. Daina, A.; Michielin, O.; Zoete, V. *Sci. Rep.* **2017**, *7*, 42717.
14. Pires, D. E. V.; Blundell, T. L.; Ascher, D. B. *J. Med. Chem.* **2015**, *58*, 4066–4072.
15. Singh, K.; Barwa, M. S.; Tyagi, P. *Eur. J. Med. Chem.* **2007**, *42*, 394–402.
16. **Arulmani, R.; Sankaran, K. R.** *Spectrochim. Acta A Mol. Biomol. Spectrosc.* **2014**, *129*, 491–498.
17. Becke, A. D. *J. Chem. Phys.* **1993**, *98*, 5648–5652
18. Frisch, M. J.; Trucks, G. W.; Schlegel, H. B.; Scuseria, G. E.; Robb, M. A.; Cheeseman, J. R.; Scalmani, G.; Barone, V.; Petersson, G. A.; Nakatsuji, H.; Li, X.; Caricato, M.; Marenich, A. V.; Bloino, J.; Janesko, B. G.; Gomperts, R.; Mennucci, B.; Hratchian, H. P.; Ortiz, J. V.; Izmaylov, A. F.; Sonnenberg, J. L.; Williams-Young, D.; Ding, F.; Lipparini, F.; Egidi, F.; Goings, J.; Peng, B.; Petrone, A.; Henderson, T.; Ranasinghe, D.; Zakrzewski, V. G.; Gao, J.; Rega, N.; Zheng, G.; Liang, W.; Hada, M.; Ehara, M.; Toyota, K.; Fukuda, R.; Hasegawa, J.; Ishida, M.; Nakajima, T.; Honda, Y.; Kitao, O.; Nakai, H.; Vreven, T.; Throssell, K.; Montgomery, J. A.; Peralta, J. E.; Ogliaro, F.; Bearpark, M.; Heyd, J. J.; Brothers, E.; Kudin, K. N.; Staroverov, V. N.; Keith, T.; Kobayashi, R.; Normand, J.; Raghavachari, K.; Rendell, A.; Burant, J. C.; Iyengar, S. S.; Tomasi, J.; Cossi, M.; Millam, J. M.; Klene, M.; Adamo, C.; Cammi, R.; Ochterski, J. W.; Martin, R. L.; Morokuma, K.; Farkas, O.; Foresman, J. B.; Fox, D. J. Gaussian 09; **2013**.
19. Lee, C.; Yang, W.; Parr, R. G. *Phys. Rev. B* **1988**, *37*, 785–789.
20. Allen, F. H.; Kennard, O.; Watson, D. G.; Brammer, L.; Orpen, A. G.; Taylor, R. *J. Chem. Soc., Perkin Trans. 2* **1987**, S1–S19.
21. Küçükgüzel, Ş. G.; Rollas, S.; Küçükgüzel, İ.; Kiraz, M. *Eur. J. Med. Chem.* **1999**, *34*, 1093–1100.
22. Domingo, L. R.; Aurell, M. J.; Pérez, P.; Contreras, R. *J. Phys. Chem. A* **2002**, *106*, 6871–6875.
23. Fukui, K. *Science* **1982**, *218*, 747–754.
24. Parthasarathi, R.; Subramanian, V.; Roy, D. R.; Chattaraj, P. K. *Bioorg. Med. Chem.* **2004**, *12*, 5533–5543.
25. Shakoor, A.; Jan, F.; Rahman, S.; Ali, M.; Ibrahim, M.; Khan, H.; Alam, A.; Khan, A.; Ali, A. *Chem. Biodiversity* **2025**, *22*, e202402096.
26. Weinhold, F.; Landis, C. R. *Chem. Educ. Res. Pract.* **2001**, *2*, 91–104.
27. Reed, A. E.; Curtiss, L. A.; Weinhold, F. *Chem. Rev.* **1988**, *88*, 899–926.
28. Lauqman, M.; Javaid, N.; Ilyas, M.; Tahir, M. N.; Ashfaq, M.; Ali, J.; Saqlain, M.; Li, H. *New J. Chem.* **2026**, DOI: 10.1039/D5NJ04171F.
29. Berman, H. M.; Westbrook, J.; Feng, Z.; Gilliland, G.; Bhat, T. N.; Weissig, H.; Shindyalov, I. N.; Bourne, P. E. *Nucleic Acids Res.* **2000**, *28*, 235–242.
30. Morris, G. M.; Huey, R.; Lindstrom, W.; Sanner, M. F.; Belew, R. K.; Goodsell, D. S.; Olson, A. J. *J. Comput. Chem.* **2009**, *30*, 2785–2791.
31. Veber, D. F.; Johnson, S. R.; Cheng, H. Y.; Smith, B. R.; Ward, K. W.; Kopple, K. D. *J. Med. Chem.* **2002**, *45*, 2615–2623.
32. Egan, W. J.; Merz, K. M.; Baldwin, J. J. *J. Med. Chem.* **2000**, *43*, 3867–3877.
33. Lipinski, C. A.; Lombardo, F.; Dominy, B. W.; Feeney, P. J. *Adv. Drug Deliv. Rev.* **1997**, *23*, 3–25.
34. Baell, J. B.; Holloway, G. A. *J. Med. Chem.* **2010**, *53*, 2719–2740.
35. Brenk, R.; Schipani, A.; James, D.; Krasowski, A.; Gilbert, I. H.; Frearson, J.; Wyatt, P. G. *ChemMedChem* **2008**, *3*, 435–444.